Interplay between H-bonding proton dynamics and Fe valence fluctuations in $Fe_3(PO_4)_2(OH)_2$ at high pressure

G. Hearne[1*], V. Ranieri[2], P. Hermet[2], J. Haines[2], O. Cambon[2], J.L. Bantignies[3], P. Fertey[4], T. Stuerzer[5], M. Poienar[6], J. Rouquette[2*]

[1]Department of Physics, University of Johannesburg PO Box 524, Auckland Park 2006, Johannesburg, South Africa

[2]ICGM, Université de Montpellier, CNRS, ENSCM, 34095 Montpellier, France

[3]L2C, Université de Montpellier, CNRS, 34095 Montpellier, France

[4]Synchrotron Soleil, L'Orme des Merisiers, Saint-Aubin, BP 48, 91192 Gif-sur-Yvette Cedex, France

[5]Bruker AXS GmbH, Ostliche Rheinbruckenstrasse 49, Karlsruhe D-76187, Germany

[6]National Institute for Research and Development in Electrochemistry and Condensed Matter (INCEMC), Renewable Energies - Photovoltaic Laboratory (LERF), Str. Dr. A. Paunescu Podeanu, nr.144, 300569, Timisoara, Timis, Romania

SUPPLEMENTAL MATERIAL

Table of Contents

* Corresponding authors: grhearne@uj.ac.za ; jerome.rouquette@umontpellier.fr

S1. Single-crystal X-ray diffraction

S1.1. Ambient pressure

As previously reported [1], $Fe_3(PO_4)_2(OH)_2$ single crystals were grown hydrothermally at low pressure and 220 °C from a mixture of $FeSO_4{\cdot}7H_2O$, $FePO_4{\cdot}7H_2O$ and H_3PO_4.

Recently, the original $P2_1/n$ space group of barbosalite was questioned, as *n*-glide plane reflection conditions ($h0l$:$h+l=2n$) were found to be violated based on TEM and single crystal X-ray diffraction (SC-XRD) [1]. A barbosalite structure with a doubled unit cell along the *c* axis in the $P2_1$ space group was proposed based on studies on a tiny single crystal (5 µm × 6 µm × 15 µm). However, the exploration of a new synthesis batch revealed bigger crystals (at least 7 times larger) which encouraged us to reinvestigate the structure of barbosalite. These bigger crystals exhibit pseudo-hexagonal unit cell parameters with a lipscombite-like structure. From a structural point of view in the literature, these two polymorphs are mainly distinguished by the existence in the case of lipscombite, of an additional non-stoichiometric iron which connects Fe^{3+}-Fe^{2+}-Fe^{3+} face-sharing FeO_6 octahedral trimers to form infinite chains along <110> [2]. Additionally, compared with barbosalite, lipscombite exhibits a higher symmetry with a tetragonal $P4_32_12$ space group. No group-subgroup relationship links the tetragonal space group to the monoclinic $P2_1/n$ symmetry of barbosalite. Our structural analysis from measurements on these two crystal types are described below.

S1.1.1 Lipscombite-like structure (bigger crystal):

A 44 µm × 47 µm × 47 µm crystal with stoichiometry $Fe_{5.72}H_2O_{20}P_4$ was characterized based on SC-XRD using ω-scans (half-sphere) for 4.91 hours on a Bruker D8 Venture diffractometer, i.e., 565 frames.

Integration was performed with the Bruker SAINT software package using a narrow-frame algorithm and resulted in a monoclinic unit cell obtained from 20695 reflections to a maximum θ angle of 44.2° (0.51 Å resolution), of which 1243 were independent (average redundancy 16.65, completeness = 100.0%, R_{int} = 2.72%, R_σ = 4.02%) and 1186 (95.41%) were greater than $2\sigma(F^2)$. A unit cell of a = 7.3672(11) Å, b = 7.4165(12) Å, c = 7.4165(9) Å, β = 119.419 (9)°, volume = 355.83(9) $Å^3$, was obtained from the refinement of the XYZ-centroids of 5811 reflections above 20 σ(I) with 6.381° < 2θ < 88.02°. Absorption corrections were performed

using the Multi-Scan method (SADABS). The ratio of minimum to maximum apparent transmission was 0.735. The calculated minimum and maximum transmission coefficients (based on crystal size) are 0.7490 and 0.7620, respectively.

The structure was solved using the Bruker SHELXTL software package, using the space group $P\ 1\ 2_1\ 1$, with Z = 2 for the formula unit, $Fe_6O_{20}P_4$. The final anisotropic full-matrix least-squares refinement on F^2 with 113 variables converged at R_1 = 6.77%, for the observed data and wR2 = 17.6% for all data. The goodness-of-fit was 1.238. The largest peak in the final difference electron density synthesis was 1.353 $e^-/Å^3$ and the largest hole was -2.829 $e^-/Å^3$ with an RMS deviation of 0.346 $e^-/Å^3$. From the final obtained model, the density was found to be 3.635 g/cm^3 and F(000) entails 376 e^-.

Inspection of the reciprocal space, Fig. 1(left), definitely shows additional reflections in agreement with the previous proposed unit cell doubling along ***c*** [1]. However, our more detailed analysis here reveals that such reflections are due to a non-merohedral twinning, as shown in Fig. S1. This prompted us, in the following sub-section S1.1.2, to re-evaluate our previous data and analysis of a smaller barbosalite single crystal [1].

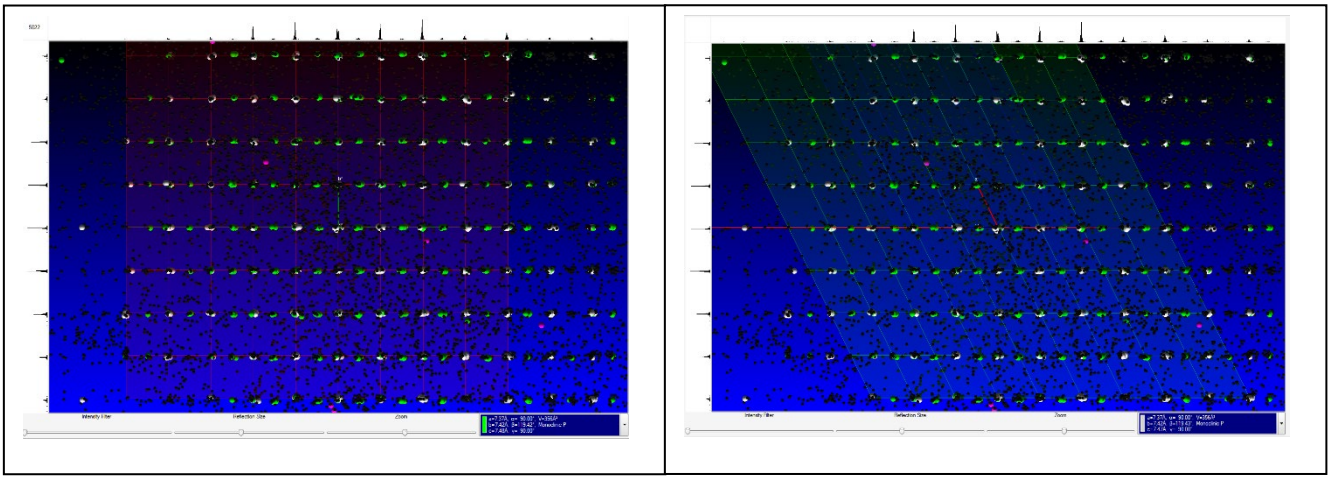

FIG. S1: Inspection of the reciprocal space showing a non-merohedral twinning with a 90° rotation angle (unit cell relationship: **a**'= -**a**, **b**'= -**b**, **c**' = **a**+**c**).

The twinned structure in this lipscombite-like crystal was thus refined based on the two domains, in a single structure in the $P2_1$ space group. There are 4 iron sites, 2 of which are non-stoichiometric and these have site occupancies of 0.489(14) and 0.511(14). They connect trimers of face-sharing FeO_6 octahedra to form infinite chains along <110> directions as already proposed in the lipscombite structure [2b, 2c]. It is particularly interesting to note that the ferrous/ferric species cannot be distinguished in this structure as the mean Fe-O distances are quite similar and could be more associated with those of intermediate valences (2.058 Å, 2.044 Å, 2.037 Å and 2.044 Å). Due to the occupancies in the non-stoichiometric iron sites mentioned above, hydrogen atoms could not be placed there in the experimentally determined structures, but are placed there based on structural relaxation in corresponding computed structures.

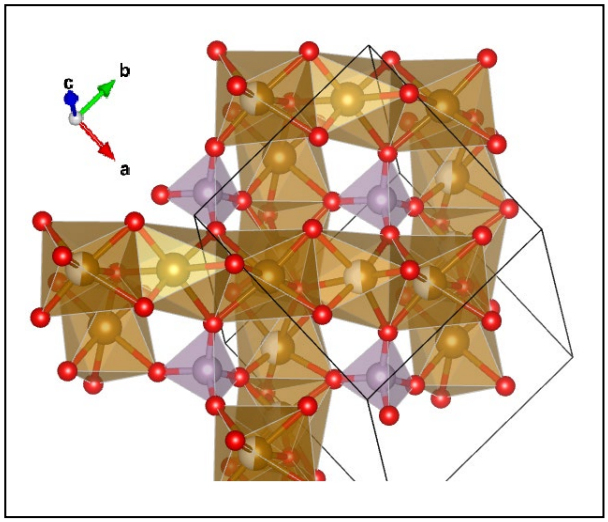

FIG. S2: Lipscombite-like structure R1=6.77%) showing some of the infinite FeO_6 chains along <110> and the 3D-connectivity of these chains by the phosphate group. Partial occupation of some of the Fe sites is indicated by a two-colour scheme.

We justify also the term "lipscombite-like" structure by the simulated X-ray powder profile obtained using the Fullprof software [3], which can be compared to previous proposed structures in the literature for lipscombite, Fig. S3. It is interesting to note the high similarity of our proposed structure with that of Song *et al.* who reported this for a pure Fe^{3+} lipscombite [4], Fig. S3(c).

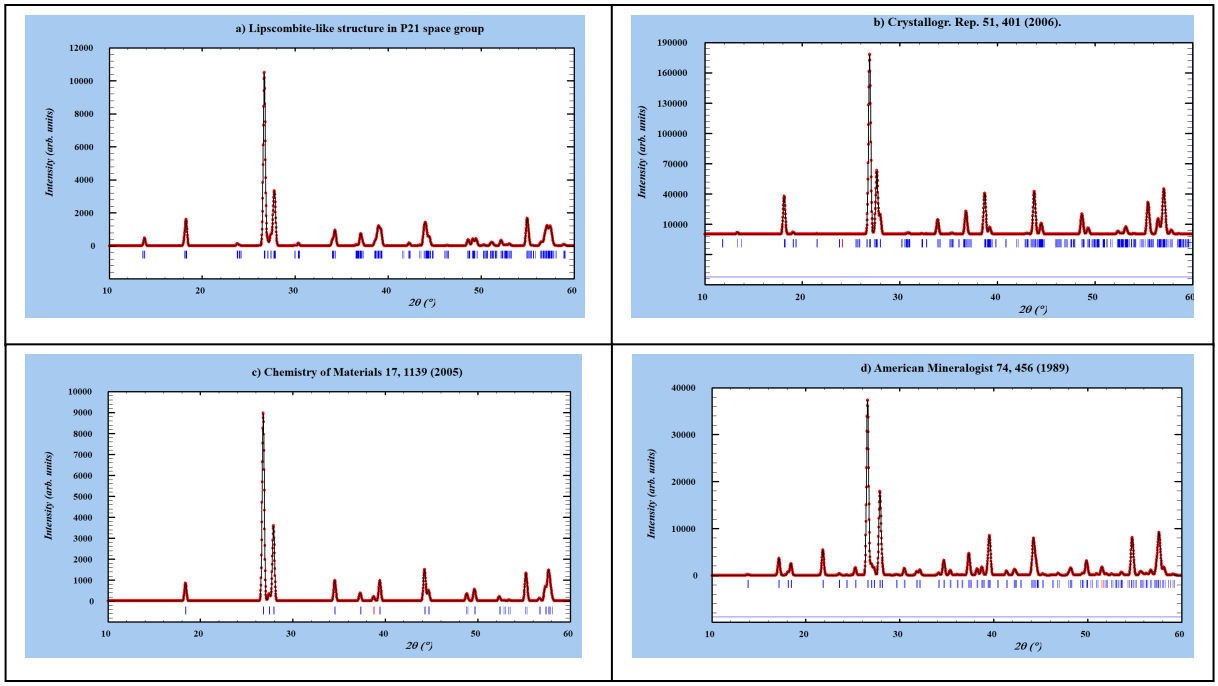

FIG. S3: Calculated powder X-ray powder profile (using Cu K_α radiation) of a) the lipscombite-like structure we obtained, compared with that from b) Yakubovich *et al.* [5] , c) Song *et al.* [4] and d) the accepted structure of Vencato *et al.* [2c].

S1.1.2 Barbosalite structure (smaller crystals):

Based on our findings in the previous sub-section S1.1.1, the data previously reported for a 5 × 6 × 15 µm^3 octahedral crystal of barbosalite [1] was reinvestigated here. As shown in Fig. S4, the previously claimed ***c*** doubling of the structure is now successfully associated with a non-merohedral twinning, involving a 90° rotation angle as found above in the lipscombite-like structure. However, as one of the domains gives weaker reflections, data reduction and structure determination was rather performed on the majority domain.

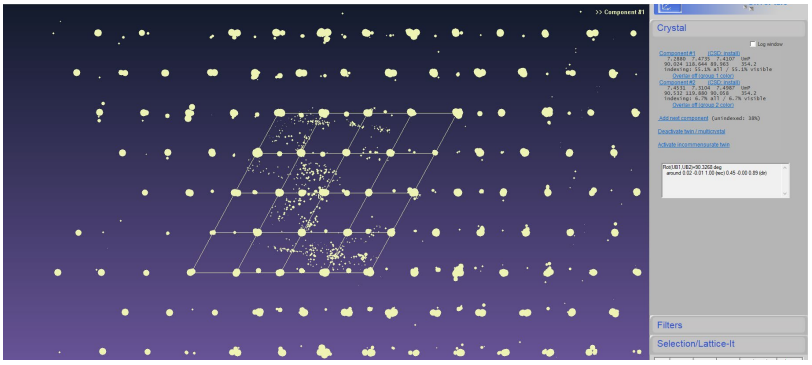

FIG. S4: Inspection of the reciprocal space of the small barbosalite crystal showing a non-merohedral twinning with a 90° rotation angle.

The barbosalite structure with a unit cell of a = 7.2873(15) Å, b = 7.4788(10) Å, c = 7.4017(13) Å, β = 118.54 (2)°, volume = 354.37(12) Å^3 is clearly still centrosymmetric with the $P2_1/n$ space-group, as either suggested by the cumulative probability distribution curves and the use of a polar twinning law in the $P2_1$ space-group solution. However, contrary to what was originally proposed [2a], the presence of an additional non-stoichiometric iron statistically connects the face-sharing FeO_6 octahedral trimers, i.e., Fe^{2+}-Fe^{3+}-Fe^{2+}, to form infinite chains along <110> directions as observed in the lipscombite-like structure, see Fig. S5 (left). There are 3 iron sites, two of which can be assigned to the ferrous and ferric species due to the mean Fe-O distances. These bond distances are: 2.0175 Å for Fe^{3+} with an abundance ratio Fe^{3+}/Fe=0.624, 2.097 Å for Fe^{2+} with an abundance Fe^{2+}/Fe = 0.333 and 2.0569 Å for the non-stoichiometric iron abundance of 0.043. This latter bond distance may seemingly be assigned to an intermediate valence state. However, note that this latter occupancy is very low and the standard deviation of the quoted bond distance exceeds those of the other iron sites. Here also, hydrogen atoms are computationally located based on structural relaxation, Fig. S5 (right). It is important to note that the non-stoichiometric iron, i.e., with its occupation of 13% (atomic percentage) on the 2*d* Wyckoff site (0.0, 0.5, 0.0), cannot be inserted in the DFT-computation. Hydrogen-atoms are normally located in the vacant octahedral volume where the additional non-stoichiometric iron atoms now reside. Such hydrogen atoms form a hydrogen bond O–H···O between the $(OH)^-$ common vertex of three octahedra and one of the oxygens of a PO_4 group, i.e., as part of Fe-O–H···O-P segments, see Fig. S5 (right panel) and Fig. 1(a) (main text). This means that in our structural description of barbosalite, the face-sharing FeO_6 octahedral trimers are separated by a vacancy involving the above-mentioned hydrogen bond or by this non-stoichiometric iron site. Thus, chains in the <110> directions may be depicted as follows: Fe^{2+}-Fe^{3+}-Fe^{2+}-**V**-Fe^{2+}-Fe^{3+}-Fe^{2+}-**$Fe^{2.5+}$**-Fe^{2+}-Fe^{3+}-Fe^{2+}-**V**-Fe^{2+}-Fe^{3+}-Fe^{2+}-**V**- …. , where **-V-** are the vacant octahedral sites separating trimers, **-$Fe^{2.5+}$-** is a non-stoichimetric iron occupation of some of these sites and site occupations are in agreement with the abundance ratios mentioned above. Note finally that different crystals were also tested at the synchrotron and confirmed the above structure of barbosalite.

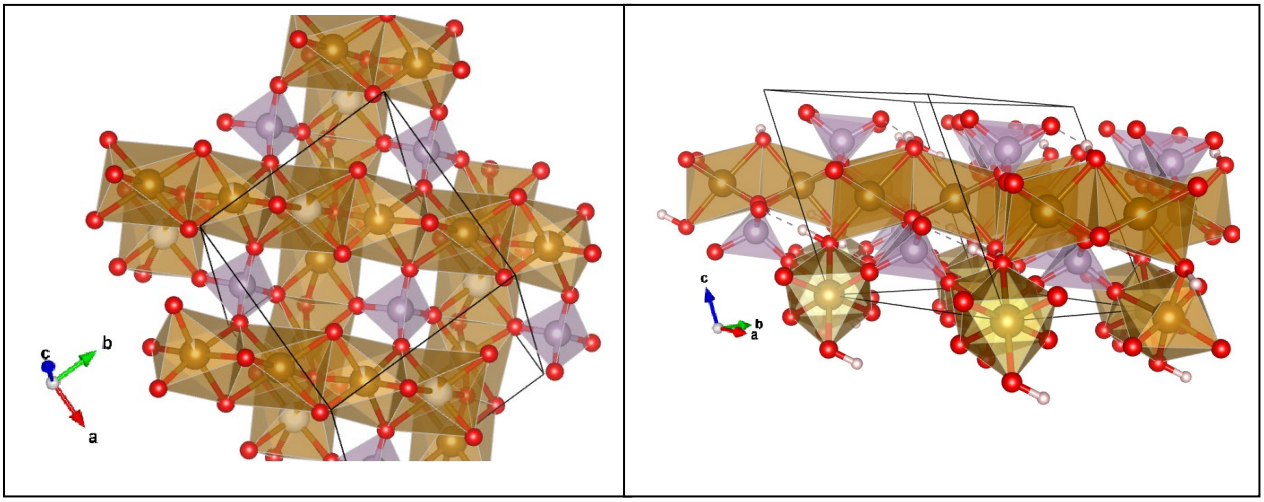

FIG. S5: Barbosalite structure (left) in the $P2_1/n$ space group (R1= 5.27 %) showing the infinite FeO_6 chains along <110>. Partial occupation of some of the Fe sites is indicated by a two-colour scheme. On the right is shown the computed barbosalite structure with H-atoms, discussed in section S2.

S1.2. High-pressure synchrotron X-ray diffraction of barbosalite

A membrane type diamond anvil cell equipped with Boehler-Almax large aperture diamonds was used for the SC-XRD experiment. A tiny crystal was placed in a 150 μm diameter cavity of a stainless steel gasket indented to a thickness of 50 μm, along with a ruby sphere and a mixture of methanol-ethanol as a pressure transmitting medium. Pressure was measured by the ruby fluorescence method [6]. Maximum pressure was limited to ~10 GPa to ensure sufficient hydrostaticity. This was ascertained from SC-XRD data quality (R_{int}, R_σ) and behavior of the ruby fluorescence manometer (line broadening effects). SC-XRD experiments (λ = 0.41640 Å) were performed on the 6-circle diffractometer on the CRISTAL beamline at SOLEIL (Saint Aubain, France). ω-scans were performed using a MARCCD detector. Indexing, data reduction and absorption corrections were performed using CrysalisPro [7]. Structure refinements were performed using SHELXL [8].

Fig. 1(b) in the main text depicts the high pressure behavior of the unit cell parameters of barbosalite, i.e., $P2_1/n$ space group. Additionally, here in Fig. S6 we also include the pressure

response of the β-angle. Whereas both unit cell parameters and the β-angle show noticeable changes at ~5 GPa, the volume-pressure behavior (inset of Fig. 1(b), main text) can be fitted using a single third order Birch-Murnaghan equation of state with K_0 = 95(2) GPa. This suggests a potential displacive phase transition is associated with this critical pressure point. At ~5 GPa, unit cell parameters tend towards the same value whereas the β-angle is still far from the symmetric-120° value of the hexagonal Bravais lattice. Such a symmetric angle β = 120° will likely be reached at ~15 GPa, from a simple linear interpolation in Fig. S6. Such a crossover could potentially either be due to another phase transition or could be the result of some pressure induced-change in the physical properties of barbosalite linked to this pseudo-symmetry, i.e., see the behavior of the Mössbauer parameters in Fig. 3(b) of the main text and Fig. S12. The emergence of such pseudo-symmetries, here at ~5 and ~15 GPa, have already been observed for example in ferroelectrics/relaxors, where in spite of cubic unit cell parameters, the actual space-group symmetry could be lower (monoclinic, triclinic) [9].

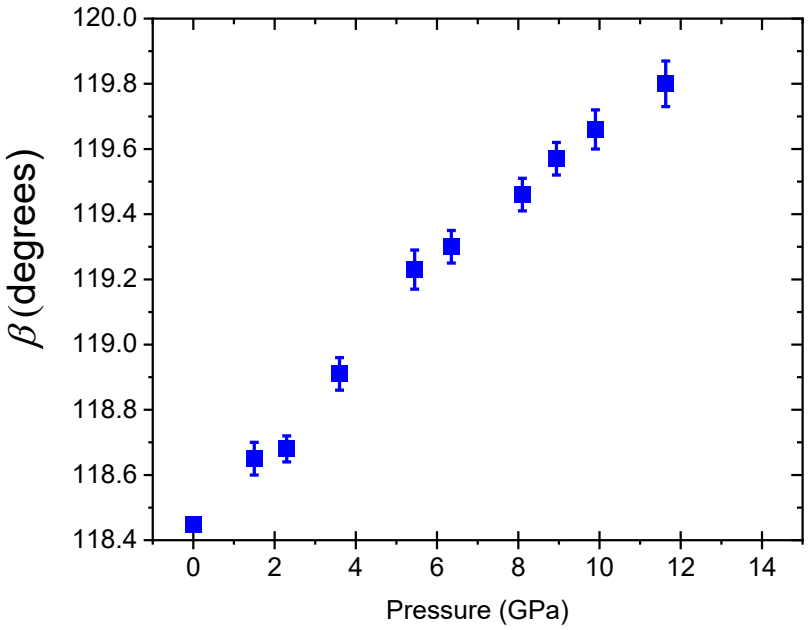

FIG. S6: Pressure dependence of the monoclinic β angle of barbosalite. Pressure dependence of unit cell parameters and volume are in Fig. 1(b) of the main text.

To identify the possible phase transition at ~5 GPa, precession images have been investigated. A closer inspection of the *hk*0 reconstruction of diffraction space shows the appearance of superlattice reflections indicative of doubling of the unit cell parameters along both ***a*** and ***b***. Note that these superlattice reflections increase in intensity during compression confirming the existence of a phase transformation. Taking into account accepted group-subgroup relationships [10], a $P2_1/n$ to *Cc* phase transition can be considered.

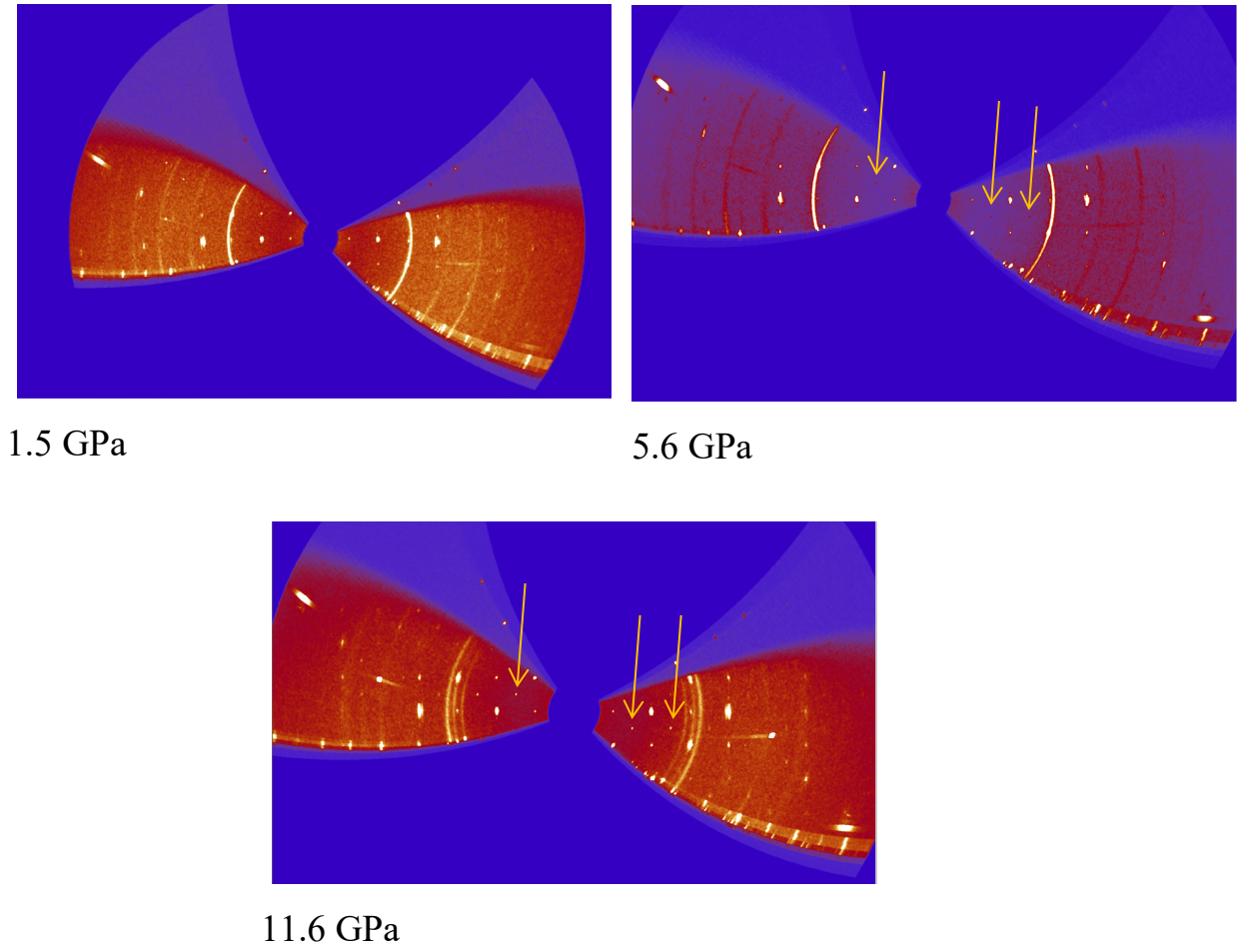

FIG. S7: *hk*0 reconstruction of the reciprocal space in barbosalite. Superlattice reflections emerging at ~5.6 GPa are highlighted by the arrows.

As superlattice reflections increase in intensity with increasing pressure the data at 9.9 GPa was used to determine the high pressure structure of barbosalite, i.e., at the highest pressure involving hydrostatic conditions. Data reduction was performed in the $2\boldsymbol{a} \times 2\boldsymbol{b} \times \boldsymbol{c}$ supercell. Note first that considering this large supercell and the low completeness of the high-pressure data, this results in a poor data quality with a $R_{int} = 41.76\%$, $R_{\sigma} = 20.51\%$. The high pressure

structure of barbosalite at 9.9 GPa was obtained using soft constraints on the distances and is shown in Fig. S8.

Eight types of iron sites (Fe-O bond lengths) can be found in this high-pressure form, four of which have an occupation of 0.5. As the data quality is not high enough, the obtained structure solution, i.e., *CIF* included in the supplemental information, cannot be further elaborated upon. Ferric iron is assigned to the equivalent of 3.5 out of 6 iron atoms occupying the eight types of iron sites. This is based on the mean Fe-O distances 2.0107 Å, 1.9702 Å each involving full site occupancies and 2.029 Å, 2.0009 Å and 2.0138 Å where site occupation is each at 0.5, yielding an abundance ratio $Fe^{3+}/Fe = 0.583$. The Fe-O bond lengths of other iron sites are 2.0668 Å, 2.0399 Å each involving full site occupancies; and 2.0543 Å for a site with an occupation of 0.5. These yield an abundance ratio $Fe^{n+}/Fe=0.4166$, best associated with intermediate valence states. This seems to be consistent with the analysis of Fe-Mössbauer data, Fig. 3(a) of the main text, which suggests inter-valence electron transfer between face-sharing octahedra and associated polaron hopping is triggered at ~10 GPa, from the preceding proton delocalization onset at lower pressure.

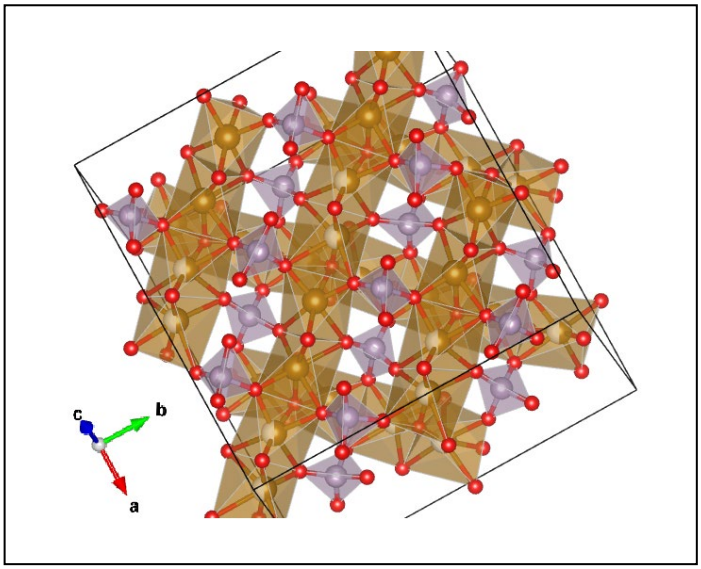

Figure S8: High-pressure structure of barbosalite obtained at 9.9 GPa in the *Cc* space group (R1=15.87%). Partial occupation of some of the Fe sites is indicated by a two-colour scheme.

S2. Computational methods

Structure relaxation and calculation of the infrared spectrum are based on the density functional theory and Perdew, Burke and Ernzerhof [11] generalized gradient approximation

(GGA), as implemented in the VASP package [12]. The interactions between ions and electrons were described by the projector augmented wave method [13]. The plane wave energy cutoff of lipscombite (resp. barbosalite) was 450 eV (resp. 500 eV) and the Brillouin zone integration was performed using a 5 × 5 × 5 (resp. 6 × 6 × 6) Monkhorst-Pack *k*-mesh [14]. To properly describe the electron correlations on Fe-atoms, the GGA plus on-site repulsion *U* method (GGA+*U*), as formulated by Dudarev *et al.* [15], was used with an effective U_{eff} of 3 eV on Fe 3*d* orbitals.

For lipscombite, we used the experimental structure, Fig. S2, as starting point and imposed a ferromagnetic order between iron atoms. We also fixed to 0.5 the occupation of Fe03 and Fe04 atoms (labels used in the included *CIF*-file). This latter change leads to a lowering of structure symmetry from $P2_1$ to $P1$. As a result of this symmetry lowering, the $P2_1$ symmetry operator is lost and results in a simplified description of the lipscombite-like structure comprising FeO_6 octahedral trimers, as in Fig. S9. For barbosalite, we used the experimental structure ($P2_1/n$ space group) reported in Fig. S5 (left panel) as a starting point without the additional non-stoichiometric iron, i.e., octahedral trimer sequences, and obtained the structure in Fig. S5 (right panel). Similar to lipscombite, a ferromagnetic order has been imposed between iron atoms. We checked that this barbosalite structure remains in the $P2_1/n$ space group even when using a $P1$ structural model without symmetry constraints.

Structure relaxation was performed at the experimental lattice parameters and only atomic positions were relaxed until a maximum atomic residual force of 0.005 eV/ Å. Dynamical matrix and Born effective charges were calculated using the linear response theory and the infrared spectrum was obtained according to the methodology previously reported [16].

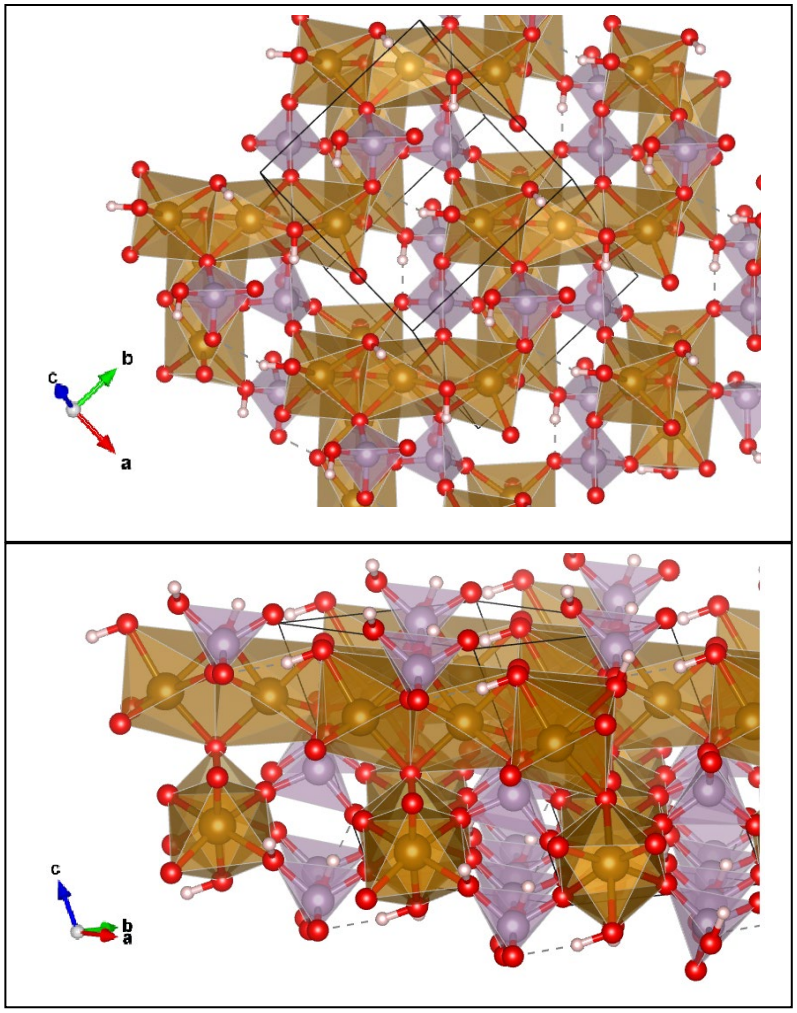

FIG. S9: Perspective views of computed lipscombite-like structure with H-atoms, as discussed in section S2.

S3. High-pressure infrared spectroscopy

Mid-infrared (IR) spectra (4000–400 cm^{-1}) were performed using a Bruker instrument IFS66v/s Fourier transform infrared spectrometer (FT-IR) equipped with a deuterated triglycine sulphate – DTGS (4000–400 cm^{-1}) detector, KBr beamsplitter and a black body source. A double condenser system (Cassegrain objectives, numerical aperture 0.4) and a diamond anvil cell were used for the pressure experiments. KBr was used as pressure transmitting medium along with barbosalite powder (tiny ground crystals). Pressure was measured by the ruby fluorescence method [6]. Limited line broadening of the ruby fluorescence bands as well as of the framework phonon modes in Fig. S10(a) attest to quasi-hydrostatic behavior up to ~16 GPa.

Infrared spectra as a function of pressure are shown in Fig. S10, along with DFT-calculated data for both $P2_1/n$ (barbosalite) and $P2_1$ (lipscombite-like) structures at ambient pressure depicted in the right-hand panel of Fig. S5 and in Fig. S9, respectively.

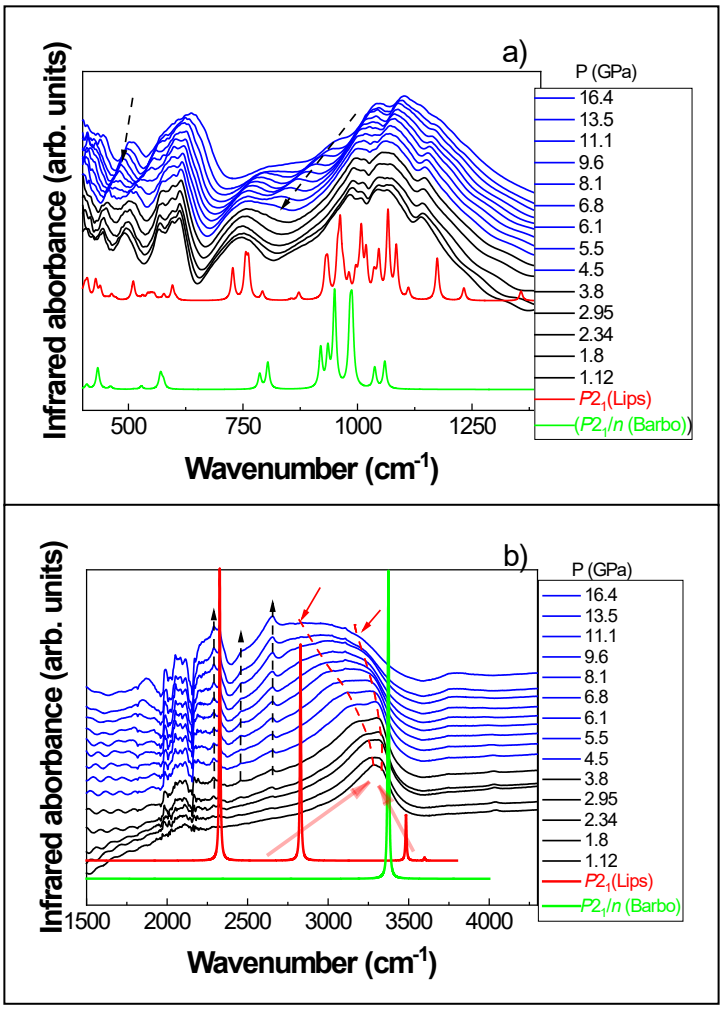

FIG. S10: Pressure evolution of barbosalite IR spectra at room temperature. a) The framework region and b) the regime of O-H vibrations. The DFT-calculated spectra at ambient pressure for both $P2_1$ (lipscombite-like) and $P2_1/n$ (barbosalite) structures are included in red and green, respectively, for comparison. In b) the transparent red arrows indicate the appreciable difference in DFT-predicted frequencies and the corresponding experimental signatures, as attributed to anharmonicity in the text. The 1950–2200 cm^{-1} region of the experimental spectra should be ignored due to the signal from the diamond anvils. Dashed arrows indicate the pressure induced change in the IR vibrational behaviour while red dashed lines show the pressure induced softening of the stretching modes.

Note that the experimental barbosalite IR spectroscopy signal near ambient pressure shown in Fig. S10(a) is much more similar to the calculated lipscombite-like spectrum than the barbosalite one. This is understood to be based on a local symmetry-breaking from the average disordered structure obtained by SC-XRD, described in sub-section 1.1.2. As previously indicated there, FeO_6 octahedral trimers in a <110> chain are separated by a vacant octahedral site involving a hydrogen bond, or such trimers in a chain are linked by a non-stoichiometric iron site. The local structure probed by IR spectroscopy is therefore lower than the $P2_1/n$ average symmetry. In the DFT-calculated IR spectrum of barbosalite, only one ν(O–H) stretching mode can be observed at about 3370 cm^{-1} whereas 4 modes are predicted in the lipscombite-like structure at 2326, 2828, 3485 and 3600 cm^{-1}, i.e. , ν(O–H) stretching modes with the participation of PO_4. The difference in frequency positions between the calculated and experimental signatures (represented by the transparent red arrows in Fig. S10(b)) could be related to the anharmonicity of modes (O-H stretching modes are usually quite anharmonic) and/or to the choice of the exchange-correlation functional (LDA or GGA).

The DFT-calculated IR vibrational signatures associated with the lipscombite-like lattice framework are used for mode assignments in the experimental spectrum of Fig. S10(a). The mode assignments are as follows [17]: i) PO_4 and FeO_6 deformation modes with the participation of the hydroxyl $(OH)^-$ are in the 450–510 cm^{-1}region, ii) deformation modes of the PO_4 tetrahedron with the participation of $(OH)^-$ are at ~600 cm^{-1}, iii) O–H bending modes with participation of the PO_4 are mainly at ~750 cm^{-1} and iv) PO_4 stretching modes with participation of $(OH)^-$ occur at ~1000 cm^{-1}.

Upon compression, the $P2_1/n$ to Cc phase transition identified by SC-XRD, sub-section S1.2, is discerned in the IR spectrum by the appearance of new vibrational modes at 817 cm^{-1} in Fig. S10(a), and the combination at 2296 cm^{-1}, 2458 cm^{-1} and 2652 cm^{-1} in Fig. S10(b). This concurs with the unit cell doubling along ***a*** and ***b***, discussed in the latter part of previous sub-section S1.2, which is expected to result in an increase in the number of vibrational bands. Also note the progressive increase in intensity of these new IR modes with increasing pressure above ~5 GPa, as previously reported for the intensity of superlattice reflections based on SC-XRD , Fig. S7.

In Fig. S10(b), the pressure induced softening of the O–H stretching modes is clearly evidenced, implying a reinforcement of the hydrogen bond of Fe-O–H···O-P structural segments with increasing pressure.

S4. High-pressure Fe Mössbauer spectroscopy (MS)

For ^{57}Fe MS pressure measurements, powdered sample derived from sources in ref. [1] has been loaded into the 250 μm diameter cavity of a Re gasket in a miniature Merrill-Basset-type DAC [18]. Initial sample thickness was in the range 20–25 μm and silicone oil was used as pressure transmitting medium. Pressures have been obtained from the *R1*-fluorescence of ruby-ball markers loaded into the sample cavity. Quoted pressures are the average values from the 5-10 % pressure distribution in the central two-thirds of the cavity. Details of the MS pressure methodology may be found in ref. [19]. This DAC was loaded onto an x-y stage enabling precise alignment with the tip of a ^{57}Co(Rh) "point" source (0.5×0.5 mm, 10 mCi) for in-house Mössbauer pressure measurements at RT in transmission geometry.

Spectrum calibration (x-axis velocity scale) was obtained by measuring Mössbauer spectra for alpha-iron metal (α-Fe) foil and sodium nitroprusside (SNP) reference absorbers.

The in-house MS measurements involved a "point" source of high specific activity leading to a broader linewidth (LW) than a conventional source. The extent of line broadening was established from measurements of the reference absorbers. Additional line broadening (extrinsic) effects arise due to pressure gradients in the DAC sample cavity and the non-hydrostatic conditions under pressure, leading to a distribution of strains in the sample. These effects of line broadening were used to decide on the fixed LW parameter value to use in the dynamical theory fitting of spectra measured at high pressure, discussed below.

Spectrum analysis was by means of *MossWinn* software [20], to extract the hyperfine interaction (HI) IS and QS parameters [21] . This has a static theory involving a superposition of Lorentzian profile signatures for Fe^{2+} and Fe^{3+} sites in the charge-ordered state, whereby HI parameters are obtained from non-linear least squares fitting of the data.

In addition, *MossWinn* also incorporates a dynamical theory of electron hopping effects on Fe^{2+} and Fe^{3+} signatures in a spectrum, e.g., when there is electron transfer between such neighbouring sites in a lattice leading to $Fe^{2+} \Leftrightarrow Fe^{3+}$ valence fluctuations. Examples of application of this theory may be found in refs. [22] and [23], based on the theory and formalism by Blume [24] involving a fluctuating Hamiltonian due to temporal changes in the Fe local environment. In using this dynamical theory to fit spectra, instantaneous values of HI parameters for the Fe^{2+} and Fe^{3+} sites as well as valence fluctuation rate ω are obtained as free parameters in attaining best fits to the lineshape of the spectral profile. Fig. S11 illustrates the

effects of valence fluctuation rate on lineshape, as obtained from simulations of spectra using the dynamical theory in the *MossWinn* package.

For the spectral analysis of data in Fig. 2(a) of the main text, fitting was initially done using the static theory (superposition of Lorentzian doublets) for a number of spectra up to ~20 GPa. Both Fe^{2+} and Fe^{3+} doublets have very similar LW values up to ~ 5 GPa. At higher pressures the Fe^{2+} component starts to broaden more than the Fe^{3+} component. Beyond ~10 GPa excessive line-broadening and distortions of the original Fe^{2+} wide-doublet profile occur, see Fig. 2(a) of the main text, whereas the Fe^{3+} narrow-doublet shows nominal line broadening up to ~10 GPa and then a further ~25 % line broadening up to ~20 GPa. This behaviour is testimony that the static theory is not applicable to spectra above several GPa.

Hence, the expectation of electron transfer between neighbouring $Fe^{2+} \rightarrow Fe^{3+}$ sites leading to valence fluctuations in the chains of Figs. 1(a) and S5 prompted us to deploy the dynamical theory mentioned above in analysing the spectra, i.e., similar to Fig. S11. In the analyses of the pressure series of measured spectra, the linewidths of Fe^{2+} and Fe^{3+} sub-components were rather fixed at values obtained from measuring the α-Fe and SNP reference samples mentioned above, in relation to when MS measurements were conducted on the sample in the DAC. Earlier low pressure MS measurements to 21 GPa involved LW = 0.31 mm s^{-1} in the analyses and later measurements beyond 21 GPa involved a different $^{57}Co(Rh)$ source and LW = 0.36 mm s^{-1} in the analyses. Thus, the dynamical theory fitting protocol used for spectral analysis in Fig. 2 involved the determination of instantaneous HI parameters (QS and IS) of Fe^{2+} and Fe^{3+} sub-components and ω valence fluctuation rate as free fitting parameters. Additional fitting parameters were fixed, viz., LW and ratio of Fe^{3+}:Fe^{2+} instantaneous abundances at 2:1 of barbosalite at ambient pressure.

Comparison of the ω parameter between when a fixed LW was used and when it was freed in the fitting, provided the y-axis error estimates in Fig. 3(a) in the main text. There are larger error bars at high pressures because resonance features become smeared and diffuse, *cf.* Fig. 2(a) and Fig. S11 where $\tau_R \sim \tau_Q$. Thus, freeing the LW parameter in the fitting yields both additional LW broadening and a correlated decrease in the ω parameter for the best fit to the spectral profile. The x-axis error bars for pressure mainly account for deviations from hydrostaticity and pressure gradients in the sample cavity.

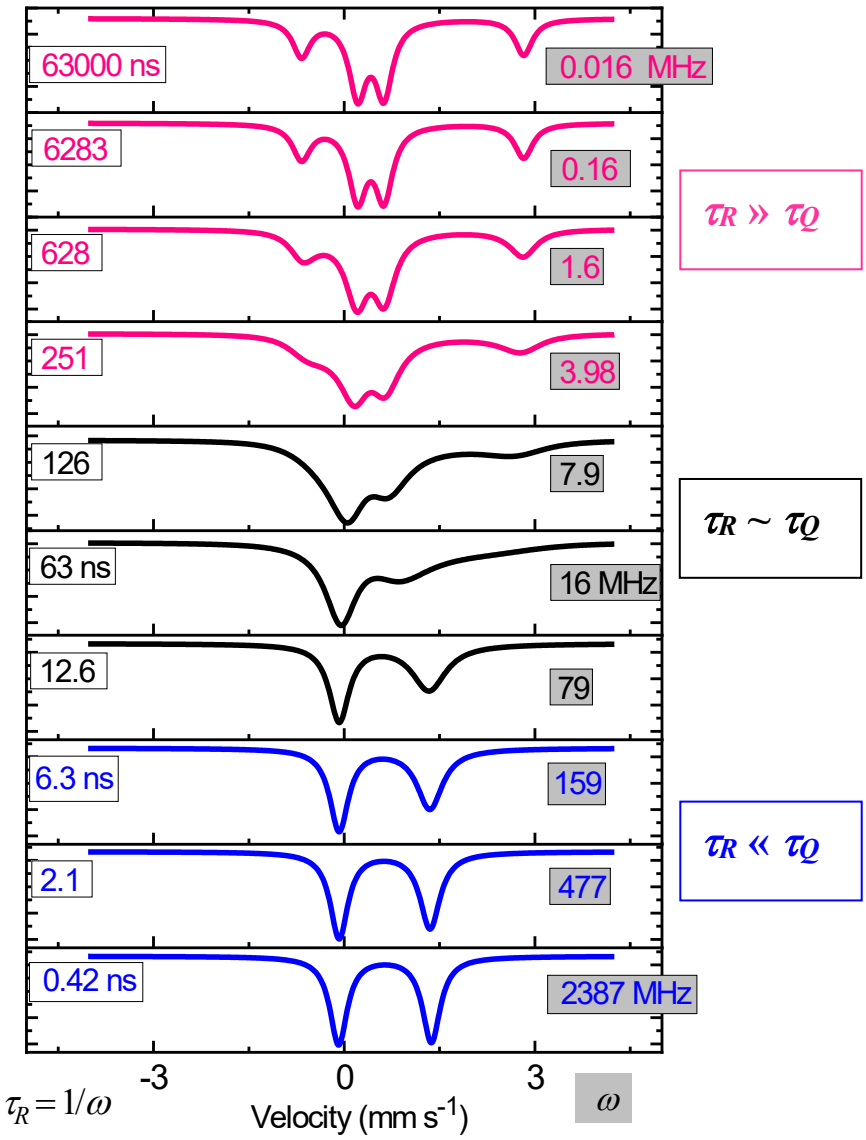

FIG. S11: Simulations of Mössbauer spectra involving varied electron hopping rates between ions of different oxidation states (e.g., $Fe^{2+} \Leftrightarrow Fe^{3+}$) or between Fe ions and the rest of the system in which it is embedded. The instantaneous HI parameters, IS and QS, for the Fe^{2+} and Fe^{3+} sites are fixed at those of barbosalite at ambient conditions [2a]. The valence fluctuation rate ω is indicated in the right column, being the fluctuation rate of the Hamiltonian changing between the forms associated with Fe^{2+} and Fe^{3+} [20, 22, 24]. The lineshape is seen to depend on the relative values of the time interval between electron transfers, $\tau_R = 1/\omega$, and quadrupole precession time $\tau_Q \sim 40$ ns [25]. Spectra evolve from the static slow relaxation regime ($\tau_R \gg \tau_Q$) to the intermediate relaxation regime ($\tau_R \sim \tau_Q$), and then to the fast relaxation regime ($\tau_R \ll \tau_Q$) where the HI parameters IS and QS of the spectral profile appear to be weighted average values of the static Fe^{2+} and Fe^{3+} values.

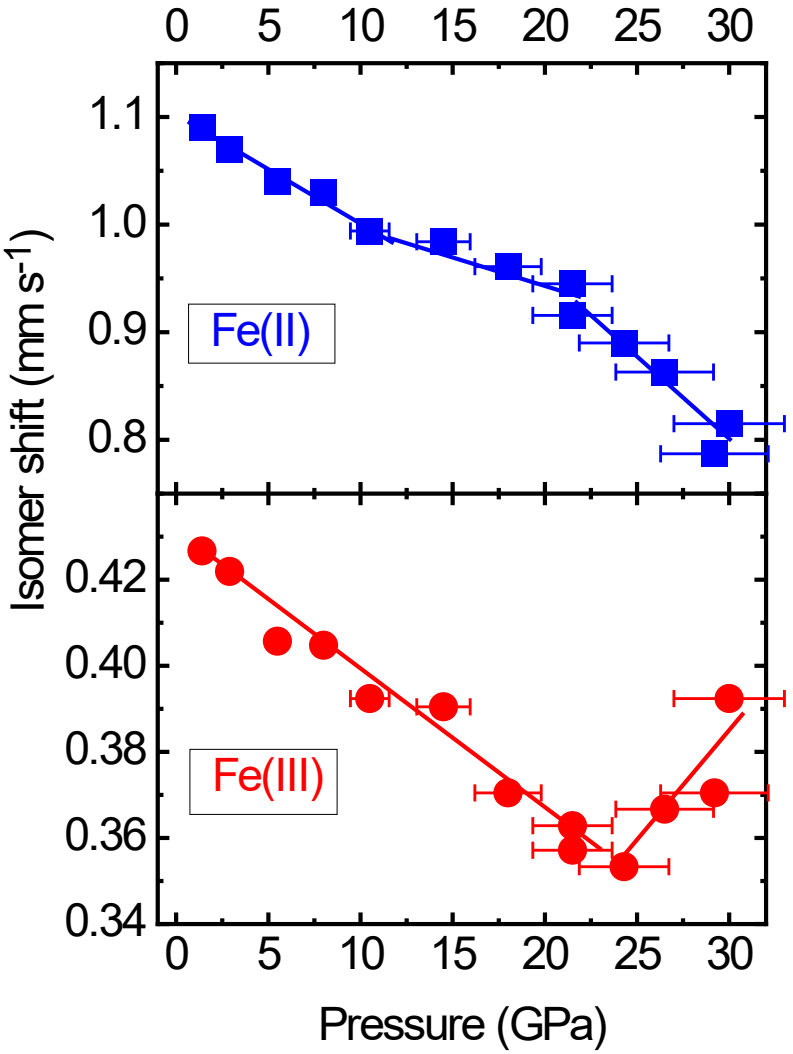

FIG. S12: Pressure evolution of instantaneous values of the isomer shift IS of the Fe^{2+} and Fe^{3+} sites (values quoted relative to α-Fe metal reference), obtained from fitting the spectra in Fig. 2(a) of the main text with the dynamical theory. Solid lines through the data points guide the eye. The decrease of IS with increasing pressure is anticipated because of the increase in *s*-electron density, $\rho_s(0)$, at the ^{57}Fe nucleus and known negative pressure dependence of IS on $\rho_s(0)$ [21, 26] . Therefore the upturn of IS at the Fe^{3+} site onset at 22-25 GPa is anomalous. There is an accompanying less conspicuous change in pressure dependence of IS of the Fe^{2+} site in the same pressure range. Instantaneous values of the other HI parameter as a function of pressure, quadrupole splitting QS, extracted from the spectral fitting are in Fig. 3(b) of the main text.

REFERENCES

[1] M. Poienar, F. Damay, J. Rouquette, V. Ranieri, S. Malo, et al., *Structural and magnetic characterization of barbosalite $Fe_3(PO_4)_2(OH)_2$*, J. Solid State Chem. **287**, 121357 (2020).

[2] a) G. Redhammer, G. Tippelt, G. Roth, W. Lottermoser, and G. Amthauer, *Structure and Mössbauer spectroscopy of barbosalite $Fe^{2+}Fe^{3+2}$ $(PO_4)_2(OH)_2$ between 80 K and 300 K*, Phys. Chem. Miner. **27**, 419 (2000); b) D. Rouzies and J. Millet, *Mössbauer spectroscopic study of synthetic lipscombite and barbosalite at room temperature*, Hyperfine Interactions **77**, 11 (1993); c) I. Vencato, E. Mattievich, and Y. P. Mascarenhas, *Crystal structure of synthetic lipscombite; a redetermination*, Am. Mineral. **74**, 456 (1989).

[3] J. Rodriguez-Carvajal, in *18th Conference on Applied Crystallography* (World Scientific Publ Co Pte Ltd, Wisla, Poland, 2000), p. 30.

[4] Y. Song, P. Y. Zavalij, N. A. Chernova, and M. S. Whittingham, *Synthesis, crystal structure, and electrochemical and magnetic study of new iron (III) hydroxyl-phosphates, isostructural with lipscombite*, Chem. Mater. **17**, 1139 (2005).

[5] O. Yakubovich, I. Steele, V. Rusakov, and V. Urusov, *Hole defects in the crystal structure of synthetic lipscombite $(Fe_{4.7}^{3+}Fe_{2.3}^{2+})[PO_4]_4O_{2.7}(OH)_{1.3}$ and genetic crystal chemistry of minerals of the lipscombite-barbosalite series*, Crystall. Rep. **51**, 401 (2006).

[6] a) A. D. Chijioke, W. J. Nellis, A. Soldatov, and I. F. Silvera, *The ruby pressure standard to 150 GPa*, J. of Appl. Phys. **98**, 114905 (2005); b) S. Klotz, J. C. Chervin, P. Munsch, and G. L. Marchand, *Hydrostatic limits of 11 pressure transmitting media*, J. Phys. D: Appl. Phys. **42**, 075413 (2009).

[7] CrysAlisPro Software System, Rigaku Oxford Diffraction, (2020).

[8] G. M. Sheldrick, *Crystal structure refinement with ShelXL*, Acta Cryst. **C71**, 3 (2015).

[9] a) J. Rouquette, J. Haines, V. Bornand, M. Pintard, P. Papet, et al., *Transition to a cubic phase with symmetry-breaking disorder in $PbZr_{0.52}Ti_{0.48}O_3$ at high pressure*, Phys. Rev. B **65**, 214102 (2002); b) J. Rouquette, J. Haines, V. Bornand, M. Pintard, P. Papet, et al., *Pressure-induced rotation of spontaneous polarization in monoclinic and triclinic $PbZr_{0.52}Ti_{0.48}O_3$*, Phys. Rev. B **71**, 024112 (2005); c) G. Fraysse, J. Haines, V. Bornand, J. Rouquette, M. Pintard, et al., *Low-symmetry phases at the tilt boundary of the $Pb(Zr_{1-x}Ti_x)O_3$ solid solution*, Phys. Rev. B **77**, 064109 (2008); d) A. Al-Zein, J. Hlinka, J. Rouquette, and B. Hehlen, *Soft Mode Doublet in $PbMg_{1/3}Nb_{2/3}O_3$ Relaxor Investigated with Hyper-Raman Scattering*, Phys. Rev. Lett. **105**, 017601 (2010).

[10] https://www.cryst.ehu.es/

[11] J. P. Perdew, K. Burke, and M. Ernzerhof, *Generalized gradient approximation made simple*, Phys. Rev. Lett. **77**, 3865 (1996).

[12] a) G. Kresse and J. Furthmuller, *Efficiency of ab-initio total energy calculations for metals and semiconductors using a plane-wave basis set*, Comp. Mat. Sci. **6**, 15 (1996); b) G. Kresse and J. Hafner, *Ab initio molecular dynamics for liquid metals*, Phys. Rev. B **47**, 558 (1993).

[13] G. Kresse and D. Joubert, *From ultrasoft pseudopotentials to the projector augmented-wave method*, Phys. Rev. B **59**, 1758 (1999).

[14] H. J. Monkhorst and J. D. Pack, *Special points for Brillouin-zone integrations*, Phys. Rev. B **13**, 5188 (1976).

[15] S. L. Dudarev, G. A. Botton, S. Y. Savrasov, C. J. Humphreys, and A. P. Sutton, *Electron-energy-loss spectra and the structural stability of nickel oxide: An LSDA+U study*, Phys. Rev. B **57**, 1505 (1998).

[16] P. Hermet, J. L. Bantignies, A. Rahmani, J. L. Sauvajol, M. R. Johnson, et al., *Far- and Mid-Infrared of Crystalline 2,2'-Bithiophene: Ab Initio Analysis and Comparison with Infrared Response*, J. Phys. Chem. A **109**, 1684 (2005).

[17] a) R. L. Frost, Y. Xi, A. López, R. Scholz, C. de Carvalho Lana, et al., *Vibrational spectroscopic characterization of the phosphate mineral barbosalite* $Fe^{2+}Fe_2^{3+}(PO_4)_2(OH)_2$ *– Implications for the molecular structure*, J. Mol. Struct. **1051**, 292 (2013); b) Q. Williams and L. Guenther, *Pressure-induced changes in the bonding and orientation of hydrogen in FeOOH-goethite*, Solid State Commun. **100**, 105 (1996).

[18] E. Sterer, M. P. Pasternak, and R. D. Taylor, *A Multipurpose Miniature Diamond Anvil Cell.*, Rev. Sci. Instrum. **61**, 1117 (1990).

[19] G. R. Hearne, M. P. Pasternak, and R. D. Taylor, *^{57}Fe Mössbauer Spectroscopy in a Diamond-Anvil Cell at Variable High Pressures and Cryogenic Temperatures*, Rev. Sci. Inst. **65**, 3787 (1994).

[20] For example MossWinn 4.0, Mössbauer spectral analysis software, by Zoltán Klencsár (see http://www.mosswinn.com/).

[21] The hyperfine interaction (HI) parameters as well as Fe site abundances are derived from fitting the spectral envelope with an appropriate static (Lorentzian sub-components) or dynamical theory. The isomer (chemical) shift IS is proportional to the *s*-electron density at the Fe nucleus and is influenced by *3d*-electron shielding. The quadrupole doublet-splitting, QS, is proportional to the aspherical distribution of surrounding electronic and nearest neighbor atomic charge. The IS, QS, and H_{hf} (from magnetically split hyperfine structure) parameters have distinct "fingerprint" values for both valences and spin states of $Fe^{2+}(3d^6)$ and $Fe^{3+}(3d^5)$.

[22] R. H. Herber and H. Eckert, *Electron hopping in FeOCl intercalation compounds: A Mössbauer relaxation study*, Phys. Rev. B **31**, 34 (1985).

[23] F. J. Litterst and G. Amthauer, *Electron delocalization in Ilvaite, a reinterpretation of its ^{57}Fe Mössbauer spectrum*, Phys. Chem. Minerals **10**, 250 (1984).

[24] M. Blume, *Stochastic theory of line shape: generalization of the Kubo-Anderson model*, Phys. Rev. **174**, 351 (1968).

[25] QS hyperfine interaction signatures will be observed provided that a complete precession of the quadrupole moment takes place before the ^{57}Fe nucleus de-excites to a ground state, i.e., $\tau_Q < \tau_N$, where $\tau_N = 140$ ns is the lifetime of the nuclear excited state. Quadrupole precession frequency $\omega_Q = (½)(eQV_{zz})/\hbar$, where V_{zz} is the maximum value of the electric

field gradient and Q the quadrupole moment. The numerator is the quadrupole (spectral doublet) splitting QS in the static limit for an axially symmetric EFG. The quadrupole precession frequency is $\omega_Q \sim 14 \times 10^7$ rad s^{-1} for QS ~ 2 mm s^{-1} and thus the corresponding precession time is $\tau_Q \sim 40$ ns. Similar arguments hold for the magnetic hyperfine interaction where the more well known Larmor precession frequency of the nuclear magnetic moment would be the main consideration.

[26] J. K. Desmarais, W. Bi, J. Zhao, M. Y. Hu, E. Alp, et al., *^{57}Fe Mössbauer isomer shift of pure iron and iron oxides at high pressure—An experimental and theoretical study*, J. Chem. Phys. **154**, 214104 (2021).